Analysis of wet pressing of paper: the three-phase model. Part I: constant air density

D. Bežanović*, C.J. van Duijn and E.F. Kaasschieter
Department of Mathematics and Computer Science, Eindhoven University of Technology, P.O. Box 513, 5600 MB Eindhoven, The Netherlands

Abstract. In this study we consider a one-dimensional three-phase model describing wet pressing of paper. Part I is devoted to the simplified case in which air is assumed incompressible. In part II we drop this assumption. The model is formulated in terms of water saturation and void ratio and it uses a material coordinate to describe spatial dependence. It also involves cross or matching conditions between the wet paper and the felt. In mathematical terms we end up with a coupled system of equations: a nonlinear diffusion equation and a first order hyperbolic equation. We present some analytical observations to explain the essential behaviour of the model and we carry out numerical experiments using an upwind and a front tracking method.

Keywords: paper pressing, parabolic-hyperbolic system, cross conditions, upwind and front tracking method.

1. Introduction

In the press-section of a paper machine, the wet web, together with one or two felts, passes through a press-nip consisting either of a pair of press rolls, or a single roll and a shoe. Water is squeezed out from the paper into the felt(s) by applying a pressure pulse. In the succeeding, drying section of the paper machine, excessive water is removed from the wet paper by evaporation, as it passes over a number of heated cylinders. The low efficiency and the high energy costs for drying are the reasons why much effort has been made to improve the press-section. Even a small improvement in the efficiency of the press-section may lead to a reduction of the drying time and therefore to a reduction of the energy consumption. Therefore much research, both experimental and theoretical, has been carried out to understand the wet pressing process. This has led to the development of new techniques such as extended nip presses, new multi-layered felts with higher permeabilities or the application of a heat flux: see for instance (Paulapuro, 2001; Singh, 1994).

Still, challenging questions remain to thoroughly understand the pressing process. Additional knowledge needs to be acquired to quan-

* Author for correspondence: e-mail: d.bezanovic@tue.nl

tify, for example, the influence of the air, the mechanical behaviour of the paper web, the magnitude and the direction of flow. Experimental approaches are seriously limited by the high processing speed of the paper (~ 10 m s^{-1}), and therefore by the small passage time ($\sim 10^{-2}$ s), and by the small length-scale of the paper thickness ($\sim 10^{-4}$ m). This motivates theoretical studies involving modelling, analysis and simulation.

In this paper we consider a three-phase (solid-water-air) model describing wet pressing of paper. It is a continuation of a previous study (Bežanović et al., 2004), where the case of complete saturation by water is considered. This simplifying assumption reduces the general three-phase model, involving a system of two coupled partial differential equations, to a single equation, allowing for a detailed analysis of global existence, uniqueness, as well as some qualitative properties of the solutions. In this study we show that the general model is of parabolic-hyperbolic nature. A particularity of our model is that the computational domain consists of two parts, corresponding to paper and felt, and that the systems are coupled across the interface through so-called cross conditions. Naturally, the coefficients of the equations and the initial conditions are discontinuous over the paper-felt interface. These facts pose a limit on the purely analytical approach. Thus we combine it with numerical computations.

We study the case of constant air density in this paper. This simplification makes the structure of the equations more clear for the mathematical discussion, while the type of system and the fundamental properties of its solutions remain the same as in the general case of non-constant air density. Here we explain in detail our analytical and numerical methods and results. Then, in the sequel of this paper (Bežanović et al., 2005), the general case of nonconstant air density is studied, using techniques proposed in this study.

This paper is organized as follows: In Section 2 we introduce the model equations, the initial and boundary conditions and the cross-conditions between paper and felt. In particular we obtain two coupled partial differential equations involving void ratio and water saturation as unknowns. These equations and some qualitative properties of the solutions are studied in Section 3. In Section 4 we discuss two different numerical methods and we present and interpret some computational results. The conclusions are given in Section 5.

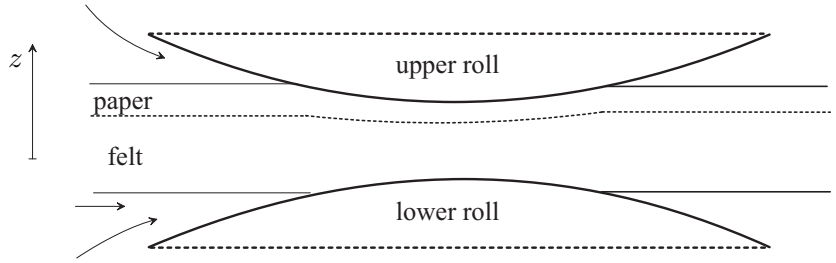

Figure 1. Sketch of the press-section of a paper machine.

2. Mathematical model

In this section we explicit our main assumptions and we present the model in terms of the void ratio and the water saturation. The approach borrows ideas from (Bežanović et al., 2004). In particular we state the equations in terms of a material coordinate.

2.1. Main assumptions

Paper and felt are considered as a system of two deformable porous layers obeying similar laws for water and air transport (Darcy) and having similar mechanical properties. Specifically, we assume that the layers exhibit elastic behaviour with a permeability that changes with deformation (porosity). Because their behaviour differs only in a quantitative way (i.e. the laws have different constants for paper and felt), we disregard the differences for the moment. This simplifies the discussion and the notation.

Having in mind the typical geometry of press-rolls and the experimental and theoretical arguments stated in (Kataja et al., 1992; Singh, 1994; Velten and Best, 2002), we consider the flow and the deformation only in transversal (vertical) direction z, obtaining a one-dimensional transversal model. Thus we disregard horizontal flow and deformation close to the beginning and the end of the nip.

The total pressure is assumed to be time-dependent and is an important input quantity of the model. The model output is, for instance, the time evolution of the thickness and the dryness of the paper.

2.2. Balance equations

To fix the computational domain we use, as in (Bežanović et al., 2004), a vertical material coordinate Z instead of the corresponding vertical spatial coordinate z, see also Figure 1. First we introduce the strain ϵ

by

$$\epsilon = \frac{\partial U}{\partial Z},$$

where U is the displacement: $U(Z,t) = z(Z,t) - z(Z,0) = z(Z,t) - Z$. In the state of compression we have

$$\epsilon^* < \epsilon \leq 0,$$

where ϵ^* is the strain corresponding to maximal deformation (zero porosity with no void space present). We consider an arbitrary control volume $V = (Z_1, Z_2)$ that follows the movement of solid particles and is fixed with respect to the material coordinates $Z = Z_1$ and $Z = Z_2$. The integral mass balance equations for solid, water and air read

$$\frac{d}{dt}\int_V (1-\phi)(1+\epsilon)\ dZ = 0, \tag{1}$$

$$\frac{d}{dt}\int_V \phi(1+\epsilon)s\ dZ - q_w(Z_1,t) + q_w(Z_2,t) = 0, \tag{2}$$

and

$$\frac{d}{dt}\int_V \phi(1+\epsilon)(1-s)\ dZ - q_a(Z_1,t) + q_a(Z_2,t) = 0. \tag{3}$$

Here ϕ denotes porosity and s water saturation. Further q_j $(j = w, a)$ denotes the discharge of phase j, relative to the solid phase. The subscript $j = w$ refers to water and $j = a$ to air.

As in (Bežanović et al., 2004), Darcy's law in material coordinates becomes

$$q_j = -\frac{k_j}{\mu_j(1+\epsilon)}\frac{\partial p_j}{\partial Z}, \tag{4}$$

where p_j is pressure, μ_j viscosity and k_j permeability of phase $j = w, a$.

The balance of total momentum yields

$$\frac{\partial p_T}{\partial Z} = 0,$$

where p_T is the total applied pressure.

2.3. State equations

The phases present in paper and felt are assumed to be incompressible with constant densities $\rho_j = const$ $(j = a, s, w)$. In the second part of this study (Bežanović et al., 2005) we drop this assumption and consider the more realistic case of compressible air. Writing Darcy's law for air assumes that air behaves as a liquid with a similar momentum

balance equation. Following (Kataja et al., 1992), we disregard capillary effects between water and air and write

$$p_a = p_w =: p_f,$$

where p_f denotes the average pressure of the water-air mixture. With this assumption, the total applied pressure p_T is distributed over the solid and fluid phases accordingly to Terzaghi's principle (Bear, 1972), implying

$$p_T = p_s + p_f, \tag{5}$$

where p_s is the effective structural pressure, see for instance (Lewis and Schrefler, 1998). Further, disregarding visco-elastic and plastic effects and considering the solid networks of the layers to behave as elastic media, we have as in (Bežanović et al., 2004)

$$p_s = p_s(\epsilon),$$

where the function $p_s(\epsilon)$ is strictly decreasing in ϵ with $p_s(\epsilon^*) = +\infty$ and $p_s(0) = 0$. Specifically, we use

$$p_s(\epsilon) = p_{s0}\left[(\epsilon - \epsilon^*)^{-q} - (-\epsilon^*)^{-q}\right], \tag{6}$$

where $p_{s0} > 0$ and $q > 0$ are given constants. Our analysis, however, does not depend on this specific form and applies to all smooth functions $p_s(\epsilon)$ having the above mentioned properties.

The permeabilities k_j in the Darcy laws (4) are, as usual (Bear, 1972), modelled as products of an intrinsic permeability k and saturation dependent relative permeabilities $k_j^r = k_j^r(s)$. The intrinsic permeability depends on the porosity to account for the influence of the deformations during passage through the press-section: $k = k(\phi)$, where k is an increasing function satisfying $k(0) = 0$. The relative permeabilities are given as functions of the saturation. Specifically, we use

$$k(\phi) = k_0 \frac{\phi^3}{(1-\phi)^2} \ (k_0 > 0, \text{ Kozeny-Carman}) \tag{7}$$

and

$$k_w^r(s) = s^2, \ k_a^r(s) = (1-s)^2. \tag{8}$$

Again we note that our analysis applies to suitable generalisations of these expressions.

The applied pressure p_T acts during passage through the nip. Denoting the passage time by t_{fin}, p_T should be such that $p_T(0) = p_T(t_{fin}) = 0$, $p_T'(0) = 0$ and $p_T(t) > 0$ for $0 < t < t_{fin}$ with a single maximum. Without loss of generality we use in this paper

$$p_T(t) = p_{T0} \sin^2\left(\frac{t}{t_{fin}}\pi\right) \quad \text{for} \quad 0 \le t \le t_{fin}. \tag{9}$$

2.4. The model

Assuming that (1) is satisfied for any control volume V and that the initial configuration is undeformed ($\epsilon = 0$), we obtain the corresponding local version of the solid mass balance:

$$\frac{\partial}{\partial t}\left((1+\epsilon)(1-\phi)\right) = 0,$$

which gives after integration

$$1 + \epsilon = \frac{1-\phi_0}{1-\phi}, \tag{10}$$

where ϕ_0 is the value of the porosity ϕ corresponding to the undeformed initial state. It is convenient to write the equations in terms of the scaled void ratio u, given by

$$u = (1-\phi_0)\frac{\phi}{1-\phi}. \tag{11}$$

One easily verifies that $\epsilon^* = -\phi_0$, that

$$u = \epsilon - \epsilon^* \quad \text{with} \quad 0 < u \leq \phi_0,$$

and that

$$\phi = \frac{u}{1-\phi_0+u}.$$

In terms of the void ratio, the structural pressure (6) becomes

$$p_s = p_s(u) = p_{s0}\left[u^{-q} - \phi_0^{-q}\right], \tag{12}$$

and the intrinsic permeability (7)

$$k = k(u) = k_0\frac{u^3}{(1-\phi_0)^2(1-\phi_0+u)}.$$

Putting the balance equations (2) and (3) in local (differential) form as well, substituting the Darcy laws (4) into the results and using the state equations from Section 2.3 in terms of u and s we obtain a coupled system of equations for u and s. In dimensionless form, with

$$x := \frac{Z}{h_0} \quad \text{and} \quad t := \frac{t}{t_{fin}},$$

where h_0 is the total thickness in terms of the material coordinate Z, see also Figure 2, this system reads

$$(us)_t = (C_w(u,s)u_x)_x, \tag{13}$$

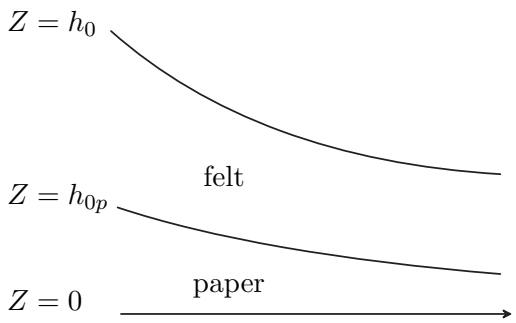

Figure 2. Two layer system.

and

$$(u(1-s))_t = (C_a(u,s)u_x)_x. \tag{14}$$

Here the indices x and t denote partial differentiation with respect to these variables. The functions C_w and C_a are given by

$$\begin{aligned} C_w(u,s) &= -\frac{t_{fin}}{h_0^2}\frac{k(u)k_w^r(s)}{\mu_w(1+\epsilon(u))}\frac{dp_s}{du} \\ &= \frac{qt_{fin}k_0p_{s0}}{h_0^2\mu_w(1-\phi_0)^2}\frac{s^2u^{2-q}}{(1-\phi_0+u)^2} =: C_{w0}s^2g(u) \end{aligned} \tag{15}$$

and

$$\begin{aligned} C_a(u,s) &= -\frac{t_{fin}}{h_0^2}\frac{k(u)k_a^r(s)}{\mu_a(1+\epsilon(u))}\frac{dp_s}{du} \\ &= \frac{qt_{fin}k_0p_{s0}}{h_0^2\mu_a(1-\phi_0)^2}\frac{(1-s)^2u^{2-q}}{(1-\phi_0+u)^2} =: C_{a0}(1-s)^2g(u). \end{aligned} \tag{16}$$

Note that

$$\frac{C_{w0}}{C_{a0}} = \frac{\mu_a}{\mu_w} = m \text{ (air-water viscosity ratio)}, \tag{17}$$

and that the function

$$g(u) = \frac{u^{2-q}}{(1-\phi_0+u)^2}$$

depends on the material through the constants q and ϕ_0.

Equations (13) and (14) hold in both the paper and felt domain where they differ only through the values of C_{w0}, C_{a0}, ϕ_0 and q. In mathematical terms, these domains are

$$\begin{aligned} \text{paper: } & Q^p = \{(x,t):\ 0 < x < x_c,\ 0 < t < 1\}, \\ \text{felt: } & Q^f = \{(x,t):\ x_c < x < 1,\ 0 < t < 1\}. \end{aligned}$$

Here $x_c = h_{0p}/h_0$ denotes the paper-felt interface, see Figure 2. The values of the constants in equations (13) and (14), when considered in the subdomains Q^p and Q^f, are denoted by the superscript i. Thus we have C^i_{j0}, ϕ^i_0, q^i and $g^i(u)$, with $j = w, a$ and $i = p, f$.

2.5. Initial, boundary and cross conditions

When solving equations (13) and (14) in the paper (Q^p) and felt (Q^f) one needs initial, boundary, and cross conditions between them.

Initial condition

We assume throughout this study that the layers are initially undeformed, i.e. $\epsilon \equiv 0$ at $t = 0$. Using (10) and (11) this gives in terms of u:

$$u(x,0) = \begin{cases} u^p_0 = \phi^p_0 & \text{for} \quad x \in (0, x_c), \\ u^f_0 = \phi^f_0 & \text{for} \quad x \in (x_c, 1). \end{cases} \tag{18}$$

In addition we assume that the initial distribution of the water saturation s is known and piecewise constant:

$$s(x,0) = \begin{cases} s^p_0 & \text{for} \quad x \in (0, x_c), \\ s^f_0 & \text{for} \quad x \in (x_c, 1). \end{cases} \tag{19}$$

In (18) and (19) the data satisfy $\phi^i_0 > 0$ and $0 < s^i_0 < 1$ for $i = p, f$.

Boundary conditions

At the boundary $x = 0$ we prescribe a 'no flow' condition, assuming that paper is in contact with an impermeable press-roll. Thus at this boundary both the water and air flux must vanish. This is ensured by the Neumann condition

$$u_x(0,t) = 0 \quad \text{for} \quad 0 < t < 1. \tag{20}$$

The fact that only one condition suffices is a consequence of the local pressure equilibrium assumption ($p_w = p_a$).

At $x = 1$ we prescribe a 'free flow' condition, assuming that the felt is in contact with a perfectly perforated press-roll, allowing for fluid flow without resistance. Thus we assume as in (Mulder and Riepen, 1994) that the fluid pressure at this boundary is constant and equal to zero. Combining this condition with (5) and (12) gives the Dirichlet boundary condition

$$\left.\begin{aligned} u(1,t) &= u_b(t) \\ \text{with} \quad p^f_s(u_b(t)) &= p_T(t) \end{aligned}\right\} \quad \text{for} \quad 0 < t < 1. \tag{21}$$

For the particular case of (9) this means that

$$u_b(0) = u_b(1) = u_0^f,\ u_b'(0) = 0 \ \text{ and } \ 0 < u_b(t) < u_0^f \ \text{ for } \ 0 < t < 1.$$

We need an additional boundary condition for s only when the fluid mixture flows back into the domain, i.e. when $u_x(1,t) > 0$. This has a physical and a mathematical explanation. In physical terms, when the fluid mixture enters the domain we need information about the content of air and water in that mixture. In mathematical terms it is a consequence of the parabolic-hyperbolic nature of the system. We therefore define

$$I^{\pm} := \{t \in (0,1) :\ u_x(1,t) \gtrless 0\},$$

and assume that

$$s(1,t) = 0 \ \text{ for } t \in I^{+}, \tag{22}$$

implying that only pure air flows back into the felt through the perforated press-roll.

Cross conditions

To match the equations across the paper-felt interface we first return to the non-dimensionless formulation. We also introduce the notation

$$[a](t) = a(h_{0p}^{+}, t) - a(h_{0p}^{-}, t)$$

for functions $a = a(Z,t)$. The superscripts $+$ and $-$ denote the limits from above (felt) and bellow (paper), respectively.

The mass balance equations (2) and (3) imply

$$[q_w](t) = [q_a](t) = 0 \ \text{ for } \ 0 < t < t_{fin},$$

expressing conservation of mass for these phases. The total momentum balance implies

$$[p_T](t) = 0 \ \text{ for } \ 0 < t < t_{fin}.$$

Applying, as in (van Duijn et al., 1995), a regularization of the absolute permeability in a neighbourhood of the paper-felt contact to the momentum balances (4), gives

$$[p_f](t) = 0 \ \text{ for } \ 0 < t < t_{fin}.$$

Hence, by (5),

$$[p_s](t) = 0 \ \text{ for } \ 0 < t < t_{fin}.$$

In terms of the dimensionless variables, these cross conditions become

$$g^f(u)s^2u_x\Big|_{(x_c^+,t)} = \frac{C_{0w}^p}{C_{0w}^f}\, g^p(u)s^2u_x|_{(x_c^-,t)}\,, \tag{23}$$

$$g^f(u)(1-s)^2u_x\Big|_{(x_c^+,t)} = \frac{C_{0a}^p}{C_{0a}^f}\, g^p(u)(1-s)^2u_x|_{(x_c^-,t)} \tag{24}$$

and, from (12),

$$p_{s0}^f\left[(u)^{-q^f}\Big|_{(x_c^+,t)} - (\phi_0^f)^{-q^f}\right] = p_{s0}^p\left[(u)^{-q^p}|_{(x_c^-,t)} - (\phi_0^p)^{-q^p}\right]. \tag{25}$$

The pressure condition implies that the void ratio u is discontinuous across the paper-felt interface, see also Figure 3. Conditions (23) and (24) imply

$$\frac{s^2}{(1-s)^2}\Big|_{(x_c^+,t)} = \frac{s^2}{(1-s)^2}\Big|_{(x_c^-,t)},$$

and thus

$$[s](t) = 0 \tag{26}$$

for all $0 < t < 1$. If we would have introduced different relative permeabilities for paper and felt, then a jump discontinuity in saturation may occur. For instance, if

$$k_w^r(s) = \begin{cases} k_{wp}^r(s) & \text{in } Q^p, \\ k_{wf}^r(s) & \text{in } Q^f, \end{cases} \quad \text{and} \quad k_a^r(s) = \begin{cases} k_{ap}^r(s) & \text{in } Q^p, \\ k_{af}^r(s) & \text{in } Q^f, \end{cases} \tag{27}$$

then we would have found

$$\frac{k_{wf}^r(s)}{k_{af}^r(s)}\Big|_{(x_c^+,t)} = \frac{k_{wp}^r(s)}{k_{ap}^r(s)}\Big|_{(x_c^-,t)} \quad \text{for } 0 < t < 1. \tag{28}$$

Generalisation (27) and (28) will be used in Section 4 as part of one of the numerical examples. Summarizing, we use (23) and (25) as cross conditions for the void ratio and (26) for the water saturation.

3. Analysis of equations

Given appropriate parameter values one has to solve equations (13), (14) in the subdomains Q^p and Q^f, subject to the initial conditions (18), (19), the boundary conditions (20), (21) and (22), and finally the cross conditions (23), (25) and (26) across the paper-felt interface.

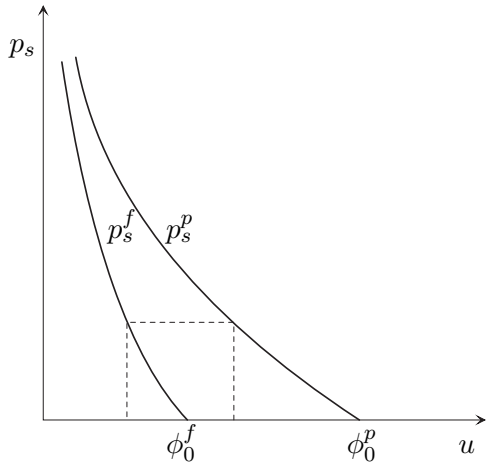

Figure 3. Pressure curves for paper and felt implying discontinuous behaviour for void ratio u across the paper-felt contact.

This is clearly not a simple task. To get some feeling for this complex system, we first consider some reduced, simpler settings.

3.1. Stationary water saturation

Direct verifications show that equations (13) and (14) become identical if the water saturation is constant and satisfies

$$C_{w0}s = C_{a0}(1-s).$$

This implies, see (17),

$$s = s^* = \frac{1}{1+m}. \tag{29}$$

Replacing s by s^*, both (13) and (14) reduce to

$$u_t = C_{w0}^i s^* \left(g^i(u)u_x\right)_x \quad \text{in} \quad Q^i,\ i = p, f. \tag{30}$$

Thus in both subdomains we end up with a nonlinear diffusion equation for the void ratio u. These equations are coupled across $x = x_c$ through the flux condition (23) (or (24), they are identical for constant saturation) and the pressure condition (25). In (Bežanović et al., 2004) we showed existence and uniqueness for the solution satisfying the piecewise constant initial condition (18) and boundary conditions (20) and (21). In addition we showed that $u_x(1,t) < 0$ (outflow) for $0 < t \leq 1/2$. For $1/2 < t \leq 1$, probably $u_x(1,t) > 0$ (inflow) does occur, in particular near $t = 1$ when the passage through the press-nip is nearly complete. The pair (u, s^*) defines a solution of the problem stated in Section 2 provided $s_0^p = s_0^f = s^*$ and $s(1,t) = s^*$ for $t \in I^+$.

In physical terms, (29) means that the saturation is frozen and that the medium behaves as if it is saturated at the value $s = s^*$.

3.2. Constant relative permeabilities

As a first step towards the understanding of equations (13) and (14) we disregard the s-dependence in the functions C_w and C_a: i.e. we replace the relative permeabilities by suitably chosen averaged values $k_w^r(s) = k_w^*$ in (15) and $k_a^r(s) = k_a^*$ in (16). Furthermore we disregard the difference between the paper and felt, except for the piecewise constant initial conditions (18) and (19). These simplifications result in the equations

$$(us)_t = k_w^* C_{w0}(g(u)u_x)_x, \tag{31}$$

$$(u(1-s))_t = k_a^* C_{a0}(g(u)u_x)_x \tag{32}$$

in $Q = \{(x,t) : \ 0 < x < 1, \ 0 < t < 1\}$. We consider solutions subject to initial conditions (18), (19) and boundary conditions (20), (21). As will become clear, boundary condition (22) is now redundant. Adding equations (31) and (32) gives for u

$$u_t = (k_w^* C_{w0} + k_a^* C_{a0})(g(u)u_x)_x \ \text{ in } \ Q. \tag{33}$$

This equation is well-known (Friedman, 1964; Ladyzhenskaya et al., 1968). It has a unique solution satisfying initial condition (18) and boundary conditions (20), (21). This solution is smooth and strictly positive for all $t > 0$. Multiplying equation (32) by $m^* := mk_w^*/k_a^*$ and subtracting the result from (31), gives

$$(us - m^* u(1-s))_t = 0 \ \text{ in } \ Q. \tag{34}$$

Hence

$$\text{or} \quad \left.\begin{array}{c} u(s - m^*(1-s))(x,t) = K(x) \\ s(x,t) = \frac{1}{1+m^*}\left(\frac{K(x)}{u(x,t)} + m^*\right) \end{array}\right\} \ \text{for} \ \ (x,t) \in Q,$$

where

$$K(x) = \begin{cases} K^p := u_0^p(s_0^p - m^*(1-s_0^p)) & \text{for} \ \ 0 < x < x_c, \\ K^f := u_0^f(s_0^f - m^*(1-s_0^f)) & \text{for} \ \ x_c < x < 1. \end{cases}$$

Thus inherited by the initial condition, s has a stationary discontinuity or shock at $x = x_c$.

The simplifying assumptions allow us to rewrite (13) and (14) in terms of a diffusion equation for u and an ordinary differential equation

in s. In the next section we show that when C_w and C_a do depend on s, it is possible to rewrite (13) and (14) in terms of a diffusion equation and a transformed hyperbolic equation. In this sense, (34) describe a degenerate case with characteristics parallel to the t-axis. This is also the reason why boundary condition (22) is redundant. It will, however, be used in the original setting of (13) and (14).

3.3. General case

In this section we introduce an analysis that applies to both the paper and felt domain. To simplify notation we drop subscripts $i = p, f$ for the moment. The key idea is to eliminate the term containing u_{xx} in equation (13) by introducing a transformation for s.

We first add equations (13) and (14) to obtain

$$u_t = \left((C_{w0}s^2 + C_{a0}(1-s)^2)g(u)u_x\right)_x . \tag{35}$$

For s given, this is to be considered as a nonlinear diffusion equation for u.

Following (Renardy, 1996), we introduce the – as yet unspecified – transformation

$$s = S(u, r) \tag{36}$$

and obtain a hyperbolic equation for the transformed variable r. Writing out (13) and substituting (36) and

$$s_t = S_u u_t + S_r r_t$$

into the result, gives

$$u_t S + u(S_u u_t + S_r r_t) = u_t(S + uS_u) + uS_r r_t = C_{w0}(S^2 g(u)u_x)_x.$$

We eliminate u_t from this expression by substituting (35). This gives

$$(S+uS_u)((mS^2+(1-S)^2)g(u)u_x)_x + \frac{1}{C_{a0}}uS_r r_t = m(S^2 g(u)u_x)_x. \tag{37}$$

In the next step we eliminate the terms containing $(g(u)u_x)_x$. This is achieved by choosing (36) such that

$$(S + uS_u)(mS^2 + (1-S)^2) = mS^2$$

or

$$uS_u = F(S) - S =: R(S). \tag{38}$$

Here $F(S)$ denotes the water fractional flow function

$$F(S) := \frac{mS^2}{mS^2 + (1-S)^2}. \tag{39}$$

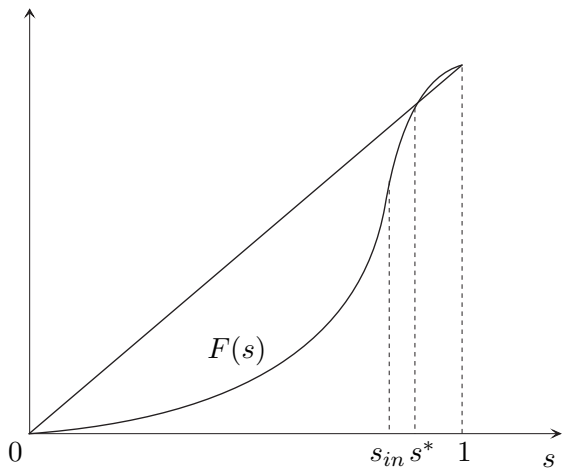

Figure 4. Sketch of the water fractional flow function $F(s)$. As indicated in this figure, we have $F(S) < S$ for $0 < S < s^*$ and $F(S) > S$ for $s^* < S < 1$. The unique interior intersection occurs at $S = s^* = 1/(1+m)$, see also (29). Further F is convex for $0 < S < s_{in}$ and concave for $s_{in} < S < 1$, with $s_{in} < s^*$.

Note that this function also arises in the well-known Buckley-Leverett equation (Leveque, 1999). A sketch of its behaviour is given in Figure 4.

Using (38) and $S_x = (S(u,r))_x = S_u u_x + S_r r_x$ in (37), we are left with

$$\begin{aligned} &\tfrac{1}{C_{a0}}\ r_t - \left[mS^2 + (1-S)^2\right] \frac{dF}{dS}(S) \frac{g(u)}{u} u_x r_x \\ &= \quad \left[mS^2 + (1-S)^2\right] \frac{dF}{dS}(S) \frac{R(S)}{S_r} \frac{g(u)}{u^2} (u_x)^2. \end{aligned} \tag{40}$$

Substituting (36) into (35) and (40) we now have a coupled system in terms of u and r: for given r, the $u-$equation (35) is second order parabolic; for given u, the $r-$equation (40) is first order hyperbolic. Before we investigate this $(u,r)-$system further, we first consider transformation (36). Since (38) is an ordinary differential equation for S in terms of u, we introduce the $r-$dependence through the initial condition. More precisely, we consider (36) as the solution of the backward initial value problem

$$(T): \begin{cases} \dfrac{dS}{du} = \dfrac{R(s)}{u} & \text{for } \ 0 < u < u_0 = \phi_0, \\ S(u_0) = r. \end{cases}$$

From (39), see also Figure 4, it follows that $R(0) = R(s^*) = R(1) = 0$ with $R(S) < 0$ for $0 < S < s^*$ and $R(S) > 0$ for $s^* < S < 1$. Hence for

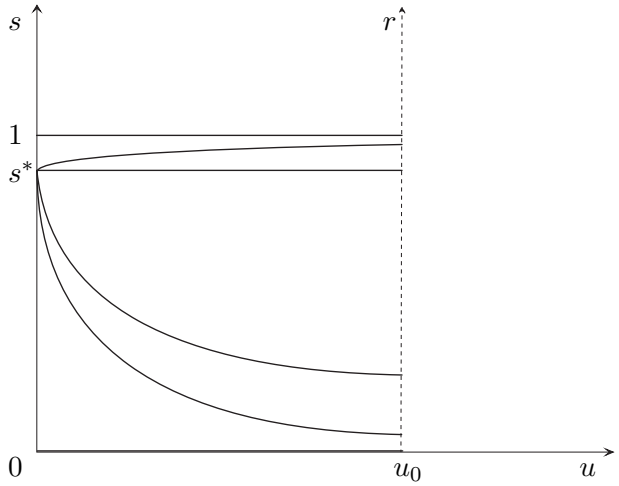

Figure 5. Sketch of solutions of Problem (T) in (u, S) space plane.

$r \in (s^*, 1)$, solutions of (T) are decreasing with decreasing u and for $r \in (0, s^*)$ solutions of (T) are increasing with decreasing u. As $u \downarrow 0$ all solutions end up at the equilibrium value $S = s^*$, except when $r = 0$ $(\Rightarrow S = 0)$ and $r = 1$ $(\Rightarrow S = 1)$. The solutions are sketched in Figure 5.

For each fixed $u \in (0, u_0)$, $s = S(u, r)$ defines a one-to-one correspondence between s and r. This is a direct consequence of uniqueness for problem (T), implying that orbits cannot touch or intersect. In fact, setting $w = dS/dr$, we have

$$\begin{cases} \dfrac{dw}{du} = \dfrac{1}{u}\dfrac{dR}{dS}(S)w \quad \text{for} \quad 0 < u < u_0, \\ w(u_0) = 1, \end{cases}$$

giving

$$w(u, r) = \exp\left(\int_{u_0}^{u} \frac{1}{S}\frac{dR}{dS}(S(\eta, r))\ d\eta\right) > 0.$$

Summarizing, we have obtained the following. Let $S(u, r)$ be the solution of Problem (T) for $0 < u \leq u_0$ and $0 \leq r \leq 1$. For given u and r this defines a unique s. Vice versa, given u and s we obtain a unique r. Using (36) in (35) we have a nonlinear diffusion equation that contains r through the transformation. Further we have for r the first order hyperbolic equation (40).

Applying the above in Q^p and Q^f means an adjustment of the constants C_{w0} and C_{a0}, of the function $g(u)$ and of the initial condition

u_0. The initial condition for r in this case is given by

$$r(x,0) = \begin{cases} s_0^p & \text{for } 0 < x < x_c, \\ s_0^f & \text{for } x_c < x < 1. \end{cases} \tag{41}$$

The hyperbolic nature of the equation for r explains why only a single cross condition is required for this variable (and thus for s) at the paper-felt interface. It also explains why we may expect discontinuous solutions or shocks for r. Since Problem (T) defines a smooth transformation, shocks in r carry over to shocks in s. Thus when treating the original system (13), (14) numerically, as we do in Section 4, we introduce shock capturing front-track and upwind methods. Employing such methods, information about the direction of the characteristics in the $(x,t)-$plane is needed. One easily verifies that both r and s have the same characteristic speed $\dot{x}(t)$. From (40) it follows that

$$\dot{x}(t) = -C_{a0}\left[mS^2 + (1-S)^2\right]\frac{dF}{dS}(S)\frac{g(u)}{u}u_x, \tag{42}$$

implying

$$\dot{x}(t) \gtrless 0 \quad \text{if} \quad u_x \lessgtr 0. \tag{43}$$

Though the characteristic speeds are the same, the location of the shocks in r and s may be different. The crucial point here is that only when dealing with smooth solutions, one is allowed to use (36) to transform the $u,s-$system into the $u,r-$system. The following example illustrates this observation.

Example 3.1. *(see also (*Smoller, 1980*)). Consider for any smooth function $f : \mathbb{R} \to \mathbb{R}$ the equation*

$$u_t + (f(u))_x = 0, \tag{44}$$

and suppose that u is a C^1 solution (continuous differentiable in x and t). Multiplying (44) by d^2f/du^2 and setting $v = df/du$, gives

$$v_t + vv_x = 0. \tag{45}$$

Hence any conservation law of type (44) can be transformed to the inviscid Burgers equation (45). The transformation from (44) to (45) fails when dealing with discontinuous solutions. This follows directly from the Rankine-Hugoniot shock conditions: in case of (44) we have

$$\textit{shock speed} = \frac{f(u_l) - f(u_r)}{u_l - u_r},$$

in case of (45) we have

$$\textit{shock speed} = \frac{1}{2}(v_l + v_r) = \frac{1}{2}\left(f'(u_l) + f'(u_r)\right).$$

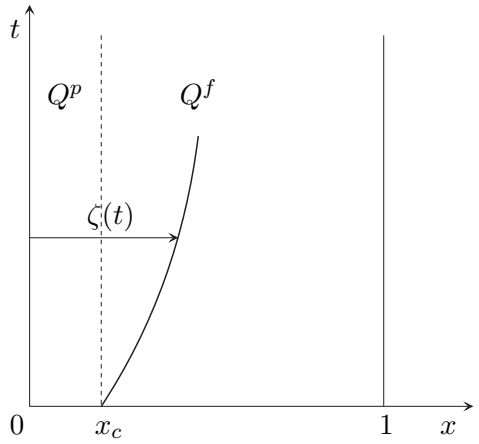

Figure 6. Sketch of shock front $x = \zeta(t)$ in Q^f.

Here u_l (u_r) denotes the value of u on the left (right) of the shock. These shock speeds only coincide for special combinations of f, u_l and u_r. In general they are different. Note that in both equations (44) and (45) the characteristic speed is given by $\dot{x} = df/du$.

Thus the formulation in terms of u and r is only useful when dealing with smooth solutions. In that case, parabolic-hyperbolic systems such as (35) and (40) have been studied in the mathematical literature (Renardy, 1996; Renardy, 1997; Ta-tsien et al., 1981). Specifically, if the medium is homogeneous (thus disregarding the difference between paper and felt) and if the initial data $u(x, 0)$ and $r(x, 0)$ is smooth, there exists a unique local (in time) solution (u, r). Using (36) this then yields a unique local (in time) solution (u, s) of (13) and (14).

Concerning the problem proposed in Section 2 we have the following generic behaviour. Initial condition (19) typically induces a shock front $x = \zeta(t)$ that moves into the felt domain Q^f, see also Figure 6.

Since u satisfies the nonlinear diffusion equation (35) in Q^f, which we write here as

$$u_t + (f_T)_x = 0 \quad \text{in} \quad Q^f$$

where f_T denotes the total flux

$$f_T = -(C^f_{w0} s^2 + C^f_{a0}(1 - s)^2) g(u) u_x, \tag{46}$$

it follows by standard arguments that both u and f_T are continuous across $x = \zeta(t)$. As a consequence ϕ and ϵ are continuous across $x = \zeta(t)$ as well. These quantities, together with u, are only discontinuous across the contact $x = x_c$. Since s is discontinuous at $x = \zeta(t)$, the flux expression (46) gives that the same is true for the derivative u_x.

Interpreting equation (13) across the shock front gives

$$[us]\frac{d\zeta}{dt} = [f_w],$$

where f_w denotes the water flux

$$f_w = -C^f_{w0} s^2 g(u) u_x. \tag{47}$$

Again $[\cdot]$ denotes the jump notation. Using the continuity of u we obtain for the speed of the saturation shock front

$$\frac{d\zeta}{dt} = \frac{1}{u(\zeta(t),t)}\frac{[f_w]}{[s]}. \tag{48}$$

Remark 3.1. *(Criteria for shocks and expansion waves)*

*Suppose s is discontinuous in space with left and right values s_l and s_r, respectively. This discontinuity can propagate either as a shock, an expansion wave or a combination of these two. It is useful to have a criterion for the type of propagating discontinuity, in particular when applying the front tracking method outlined in Section 4. Because of the convex-concave nature of $F(s)$, we can not apply arguments based on the crossing or diverging of characteristics directly, see for instance (*Leveque, 1999*, p. 48). However if $s < s_{in}$, the inflection point of $F(s)$ – see again Figure 4, we are effectively dealing with the convex part of F, which allows us to use the arguments based on the direction of the characteristics.*

First write the characteristic speed of s and r (42) as

$$\dot{x}(t) = \frac{f_T}{u}\frac{dF}{dS}(S),$$

where f_T is the total flux given by (46). Since f_T/u is continuous, we are only concerned with its sign. If $s_l, s_r < s_{in}$ the following criteria hold:

1. $s_l > s_r,\ f_T > 0 \Rightarrow$ *discontinuity propagates as a shock wave;*
2. $s_l < s_r,\ f_T > 0 \Rightarrow$ *discontinuity propagates as a expansion wave;*
3. $s_l > s_r,\ f_T < 0 \Rightarrow$ *discontinuity propagates as a expansion wave;*
4. $s_l < s_r,\ f_T > 0 \Rightarrow$ *discontinuity propagates as a shock wave.*

Analogous criteria hold when $s_l, s_r > s_{in}$.

Typical values of s in the numerical examples considered in Section 4 are bellow s_{in}, throughout $Q^p \cup Q^f$. Our application is such that $s^p_0 > s^f_0$. Hence initially $s_l > s_r$. Furthermore $f_T > 0$ (fluids flow from paper to felt), at least up to $t = 1/2$. Consequently we are dealing with case 1 at least up to $t = 1/2$.

4. Computational methods and examples

In this section we first introduce and explain two numerical methods we are going to use. Then we apply these methods to compute numerical solutions of two examples.

There are several possible approaches to find a numerical solution of our model. For instance, one can either try to find a numerical solution of the system (13) and (14) or of the transformed system (35) and (40). The advantage of the second approach is that the the system is rewritten into the standard parabolic-hyperbolic form, and the standard methods for parabolic and hyperbolic equations can be applied. The disadvantage of this approach is that the equation for r is not in divergence form and that this procedure would involve additional computation of the numerical solution $s = S(u, r)$ of Problem (T). In addition, as it was mentioned in Section 3.3, the $r-$equation gives in general the wrong speed of the propagating shock. These are the reasons to develop a suitable numerical methods for system (13)–(14).

We write system (13)–(14) in the following form (omitting unnecessary subscripts $i = p, f$):

$$(us)_t + (f_w)_x = 0, \tag{49}$$

$$(u(1-s))_t + (f_a)_x = 0. \tag{50}$$

Here the air flux f_a is given by $f_a = f_T - f_w$, where the total flux f_T and the water flux are given by (46) and (47), respectively. On the contrary to the specific choices for relative permeabilities $k_w^r(s)$ and $k_a^r(s)$ used in Sections 2 and 3, the numerical methods will be applicable to any choices of these functions. The specific choices for $k_w^r(s)$ and $k_a^r(s)$ will be specified later, in Section 4.3.

One direct way of discretizing system (49)–(50) would be to apply the standard finite volume method for spatial discretization combined with the explicit Euler method for time integration. However, the corresponding numerical solution of s contains spurious oscillations near the discontinuity. These effects come from the parabolic-hyperbolic nature of the system (that is hidden in the above form) and the fact that all spatial derivatives are approximated by central differences. To avoid these unwanted effects we will apply a suitable upwinding with respect to s, as it will be explained in the next subsection.

4.1. $s-$UPWIND METHOD

We divide the segment $[0, 1]$ into N_x equal control volumes (cells) $V_1, V_2, ..., V_{N_x}$ of size (length) $\Delta x = 1/N_x$, with centers in the points

$x_1, x_2, ..., x_{N_x}$, see Figure 7. Furthermore we split the time interval $[0,1]$ into N_t equal time steps, i.e. we take $0 = t^0 < t^1 < \cdots < t^{N_t} = 1$, such that $t^{n+1} - t^n = \Delta t = 1/N_t$, $n = 0, ..., N_t - 1$. We assume that $u_j^n \approx \int_{V_j} u(x, t^n)\, dx$ and that the paper-felt interface coincides with the interface between cells $V_{N_c-1/2}$ and $V_{N_c+1/2}$. Finally we define interface points $x_{1/2} = 0$ and $x_{j+1/2} = x_j + \Delta x/2$, $j = 1, ..., N_x$.

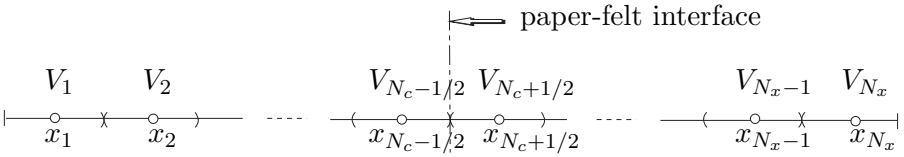

Figure 7. Grid points.

Integration of (49) and (50) over the control volume V_j for $t = t^n$, combined with explicit Euler approximation of the time derivative, gives

$$u_j^{n+1} s_j^{n+1} = u_j^n s_j^n + \frac{\Delta t}{\Delta x}\left(-(f_w)_{j+1/2}^n + (f_w)_{j-1/2}^n\right),$$

$$u_j^{n+1}(1 - s_j^{n+1}) = u_j^n(1 - s_j^n) + \frac{\Delta t}{\Delta x}\left(-(f_a)_{j+1/2}^n + (f_a)_{j-1/2}^n\right).$$

The next step is to approximate the fluxes at the cell interfaces, given by

$$(f_j)_{j\pm1/2}^n = -g(u)_{j\pm1/2}^n k_j^r(s)_{j\pm1/2}^n (u_x)_{j\pm1/2}^n,\ j = w, a.$$

We approximate $(u_x)_{j+1/2}^n$ by $(u_{j+1}^n - u_j^n)/\Delta x$ and $(u_x)_{j-1/2}^n$ by $(u_j^n - u_{j-1}^n)/\Delta x$. Further we take $g(u)_{j-1/2}^n = (g(u_{j-1}^n) + g(u_j^n))/2$ and $g(u)_{j+1/2}^n = (g(u_j^n) + g(u)_{j+1}^n)/2$. Finally, using (43) we approximate $k_{j\pm1/2}^r(s)$ at the interfaces between control volumes in an upwind fashion:

$$k_j^r(s)_{j-1/2}^n = \begin{cases} k_j^r(s_{j-1}^n) \text{ if } u_{j-1}^n \geq u_j^n, \\ k_j^r(s_j^n) \text{ if } u_{j-1}^n < u_j^n, \end{cases} \quad j = w, a,$$

end similarly with $k_j^r(s)_{j+1/2}^n$.

Approximations of initial and boundary conditions

Initial conditions imply $s_j^0 = s_0(x_j)$ and $u_j^0 = u_0(x_j)$, for $j = 1, ..., N_x$. The boundary condition at $x = 0$ gives $(f_w)_{1/2}^n = (f_a)_{1/2}^n = 0$, for $n = 0, ..., N_t$. The boundary condition at $x = 1$ gives $u_{N_x+1/2}^n =$

$u_b(t^n)$, for $n = 0, ..., N_t$. In addition, we have $s^n_{N_x+1/2} = s_b(t^n)$ whenever $u^n_{N_x} < u^n_{N_x+1/2}$.

Approximations of cross conditions

In order to discretize the cross conditions, for each time step $t = t^n$ we introduce four interface variables, as left and right states of u and s at the paper-felt interface: u^n_p, u^n_f, s^n_p and s^n_f. Straightforward discretization gives three conditions:

$$p_{sp}(u^n_p) = p_{sf}(u^n_f), \tag{51}$$

$$\begin{aligned}(f_j)^n_{N_c} : &= -C^p_{w0} g^p(u^n_p) k^{rp}_j(s^n_p)(u^n_p - u^n_{N_c-1/2}) \\ &= -C^f_{w0} g^f(u^n_f) k^{rf}_j(s^n_f)(u^n_{N_c+1/2} - u^n_f),\ j = w, a. \end{aligned} \tag{52}$$

In addition to three cross conditions (51)–(52) we have the following one: if the flow is from left to right (paper to felt) then we take s^n_p to be equal to the neighbouring upwind value, $s^n_{N_c-1/2}$, otherwise we take $s^n_f = s^n_{N_c+1/2}$. On this way the four interface variables are in general uniquely determined. The mathematical background of the last condition lies in the following fact: s and r depend from the values from one side and, knowing the sign of their characteristic speed (42), these unknowns can be approximated in an upwind maner (see also Section 3.3).

We have just seen how we numerically solve the interface problem for new time level $t = t^{n+1}$, knowing the approximations for $t = t^n$. Since the procedure depends on the direction of the flow (sign of the fluxes) at the paper-felt interface, we need a criterion for this sign. As it follows from the following lemma, this sign is determined by the relation between the the values of structural pressure in the neighbouring cells of the interface.

Lemma 4.1. *We have following equivalence:*

$$(f_w)^n_{N_c} > 0 \Leftrightarrow p^p_s(u^n_{N_c-1/2}) < p^f_s(u^n_{N_c+1/2}).$$

Proof. Pressure condition (51) gives $u^n_f = \psi(u^n_p)$, where $\psi = (p^f_s)^{-1} \circ p^p_s$ is an increasing function (composition of two decreasing functions). Flux conditions (52) yield

$$\begin{aligned}&\operatorname{sgn}(-(f_w)^n_{N_c}) = \operatorname{sgn}(u^n_p - u^n_{N_c-1/2}) = \operatorname{sgn}(u^n_{N_c+1/2} - u^n_f) \\ =\ &\operatorname{sgn}(\psi(\psi^{-1}(u^n_{N_c+1/2})) - \psi(u^n_p)) = \operatorname{sgn}(\psi^{-1}(u^n_{N_c+1/2}) - u^n_p).\end{aligned}$$

This yields implications

$$(f_w)^n_{N_c} > 0 \Rightarrow u^n_p < u^n_{N_c-1/2} \Rightarrow \psi^{-1}(u^n_{N_c+1/2}) < u^n_p.$$

Consequently $\psi^{-1}(u^n_{N_c+1/2}) < u^n_{N_c-1/2}$ and thus
$p^p_s(u^n_{N_c-1/2}) < p^f_s(u^n_{N_c+1/2})$.

Similarly $(f_w)^n_{N_c} \leq 0$ implies $p^p_s(u^n_{N_c-1/2}) \geq p^f_s(u^n_{N_c+1/2})$, which completes the proof of the lemma.

4.2. Front tracking method

The $s-$upwind method is one of the, so-called front capturing method. These methods are robust since they are able to catch the shocks anywhere in the domain, and they avoid spurious oscillations by means op upwinding. However, the numerical solutions obtained by these methods differ significantly from real solutions near the shocks, due to numerical diffusion.

To obtain the real shape of the shock and to follow and illustrate the qualitative properties of the solutions explained in Section 3, we develop a front tracking method. Naturally, this method is applied if the criteria from Remark 3.1 imply existence of a shock. The position of the shock is tracked using the shock conditions that follow from the conservation laws. At the position of the shock an additional moving grid point x^n_s is introduced. As it was explained in Section 3.3, u and f_T are continuous across the shock and thus they have (single) values at this point, u^n_s and f^n_{Ts}, respectively, while s has a left and right value, s^n_{sl} and s^n_{sr}, respectively. We apply this procedure only in the case when the combination of initial values u and s imply the crossing of characteristics and thus the appearance of the shock.

Let us assume that the following values at $t = t^n$ are known: u^n_j and s^n_j for $j = 1, ..., N_x$, u^n_s, f^n_{Ts}, s^n_{sl} and s^n_{sr}, see Figure 8. We assume that all fluxes are positive in V_j i.e. that the flow is 'from left to right' and thus we take $k^r_a(s)^n_{j-1/2} = k^r_a(s^n_{j-1})$ and $k^r_a(s)^n_{j+1/2} = k^r_a(s^n_{sr})$.

The shock speed is given by (48), implying a discrete condition

$$x^{n+1}_s = x^n_s + \Delta t \left(\frac{f^n_{Ts}}{u^n_s} \frac{\frac{k^r_w(s^n_{sr})}{k^r_w(s^n_{sr})+k^r_a(s^n_{sr})} - \frac{k^r_w(s^n_{sl})}{k^r_w(s^n_{sl})+k^r_a(s^n_{sl})}}{s^n_{sr} - s^n_{sl}} \right). \tag{53}$$

Initially ($t = t^0$) we have $x^0_s = x_{N_c}$, since we follow the shock that originates at the interface.

Consider now the situation for $t = t^{n+1}$. Values s^{n+1}_{sl} and s^{n+1}_{sr} are approximated by the values of s at $t = t^n$ in the closest points from the

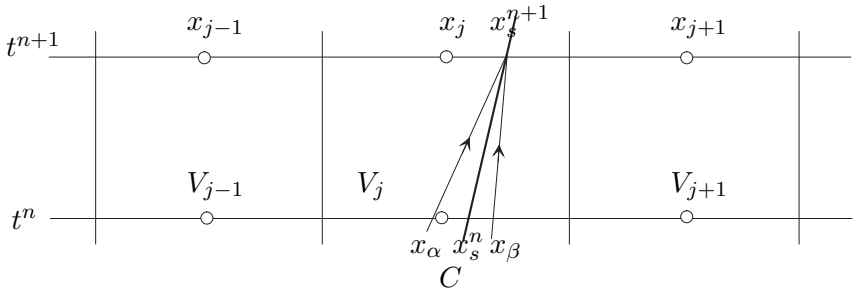

Figure 8. Front tracking method; C is the approximation of the shock curve.

same side of the shock curve: $s_{sl}^{n+1} \approx s_j^n$ and $s_{sr}^{n+1} \approx s_{j+1}^n$, see Figure 8. Similarly as in Section 4.1, these approximations are motivated by the fact that s and r depend on the upwind values along the characteristics (sketched also in Figure 8), and that two characteristics from each side of the shock meet at the point (x_s^{n+1}, t^{n+1}).

Now u_s^{n+1} is computed using the condition for continuity of water flux

$$k_w^r(s_{sl}^{n+1})\frac{u_s^{n+1}-u_j^{n+1}}{x_s^{n+1}-x_j} = k_w^r(s_{sr}^{n+1})\frac{u_{j+1}^{n+1}-u_s^{n+1}}{x_{j+1}-x_s^{n+1}},$$

and one can easily check that this condition implies also the continuity of the air flux.

4.3. Numerical examples

We consider two numerical examples. The following approximations of the functions are common for both examples: $p_T(t) = 5$ MPa $\sin^2(t)$, $t \in [0,1]$, $\mu_w = 1 \cdot 10^{-3}$ kg m^{-1}s^{-1}, $\mu_a = 1.8 \cdot 10^{-5}$ kg m^{-1}s^{-1}. The values of used parameters are given in Table I.

The numerical examples differ only in the choice of relative permeability functions. We take, for $i = p, f$,

$$\text{Ex. 1}: \begin{cases} k_w^{r\,i}(s) = s^2, \\ k_a^{ri}(s) = (1-s)^2, \end{cases} \quad \text{Ex. 2}: \begin{cases} k_w^{r\,i}(s) = s^{\frac{2+3\lambda_i}{\lambda_i}}, \\ k_a^{ri}(s) = (1-s)^2(1-s^{\frac{2+\lambda_i}{\lambda_i}}). \end{cases}$$

So, Example 1 corresponds to the same relative permeabilities (as used in Sections 2 and 3), while Example 2 corresponds to the general case, when relative permeabilities for paper and felt are different (here we take Brooks-Corey functions, see (Helmig, 1997) for instance).

The numerical solutions for Example 1 are given in Figure 9. Note that in Figure 9(b) the time t can be considered as a scaled horizontal (longitudinal) coordinate.

Table I. Parameter set used in computations.

parameter		*Paper*	*Felt*
u_0	$[\cdot]$	0.55	0.45
s_0	$[\cdot]$	0.75	0.45
k_0	$[\mathrm{m}^2]$	$5 \cdot 10^{-15}$	$1.7 \cdot 10^{-14}$
p_{s0}	[MPa]	0.23	0.5
q	$[\cdot]$	4	3.5
λ	$[\cdot]$	2	1.8
h_0	[mm]	0.17	1.47

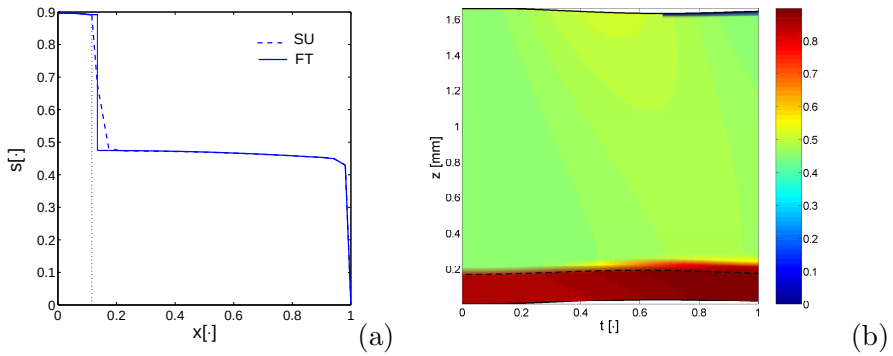

Figure 9. Computational results of Example 1. (a) Final distribution of saturation s computed by s-upwind (SU) and front tracking (FT) methods. (b) Saturation in spatial coordinates.

To compete the two numerical methods, we give the final distribution of s computed by both methods in the Figure 9(a). Figure 9(b) displays s in spatial coordinate z. The scaled material coordinate x which is used in the computations is transformed into the spatial coordinate z using

$$z(x,t) = h_0 \int_0^x (1 + \epsilon(\eta, t))\, d\eta = h_0 \int_0^x (1 + u(\eta, t) - u_0)\, d\eta.$$

So, in fact the right Figure displays not only s, but also u through the computed geometry (compression) of the domain. One can understand the time t on this figure as the horizontal spatial direction. This assumes that the process is homogenous in horizontal direction. With this interpretation, this figure represents also the corresponding two-dimensional cross section of the press nip, which is sketched also in Figure 1.

In Figures 10, 11 and 12 we give numerical solutions of Example 2. In this more general case, s has two discontinuities in space: one at the interface and another inside the felt domain, see Figure 11. The interface discontinuity is natural and expectable, arising from different relative permeability functions and the arguments of mass conservation. The second discontinuity comes from the hyperbolical nature of the equations in s and the fact that the initial values of s for paper and felt are (in general) not in equilibrium, causing an initial shock. Note that with this new choice of relative permeabilities the criterion for existence of the shock, analogous to that from from Remark 3.1, can be derived. Further, $s(1,\cdot)$ also contains an expansion wave near the right boundary. Note also that along the boundary line $x = 1$, s has a discontinuity corresponding to the moment when pure air starts to flow into the felt.

In the expansion phase, when $u_x(1,t) > 0$ and $s(1,t) = 0$, case 3 from Remark 3.1 is satisfied. Therefore an expansion wave near the right boundary is formed, see Figure 12.

The s-upwind method is by its construction (mass) conservative. The front tracking method is also conservative, since the condition (53) actually represents the mass conservation. Besides, as we can see, opposite to the s-upwind method, where mesh refinement is needed to produce a better approximation of the shock, the front tracking method produces the exact shape of the shock with a small number of grid points.

The driving force in the proposed model is a given total pressure transformed to a Dirichlet boundary condition for u. This boundary condition causes in the first part of press nip flow from paper to felt ($u_x < 0$). In the second part of this paper (Bežanović et al., 2005) (compressible air case combined with 'no flow' boundary conditions) the driving force will be the source term arising from the compression of air. This is the fundamental difference between these two models.

The calculated dryness gain of the paper is 2.4% in Example 1 and 2% in Example 1, where dryness is defined as mass of solid particles per mass of complete medium. However, we address in more details these questions of engineering interest (dryness gain, thickness, compression, etc.) in the second part of this paper (Bežanović et al., 2005), where the more realistic model is studied.

5. Conclusions

In this paper we have derived a three-phase model for wet pressing of paper. It consists of a pair of coupled partial differential equations.

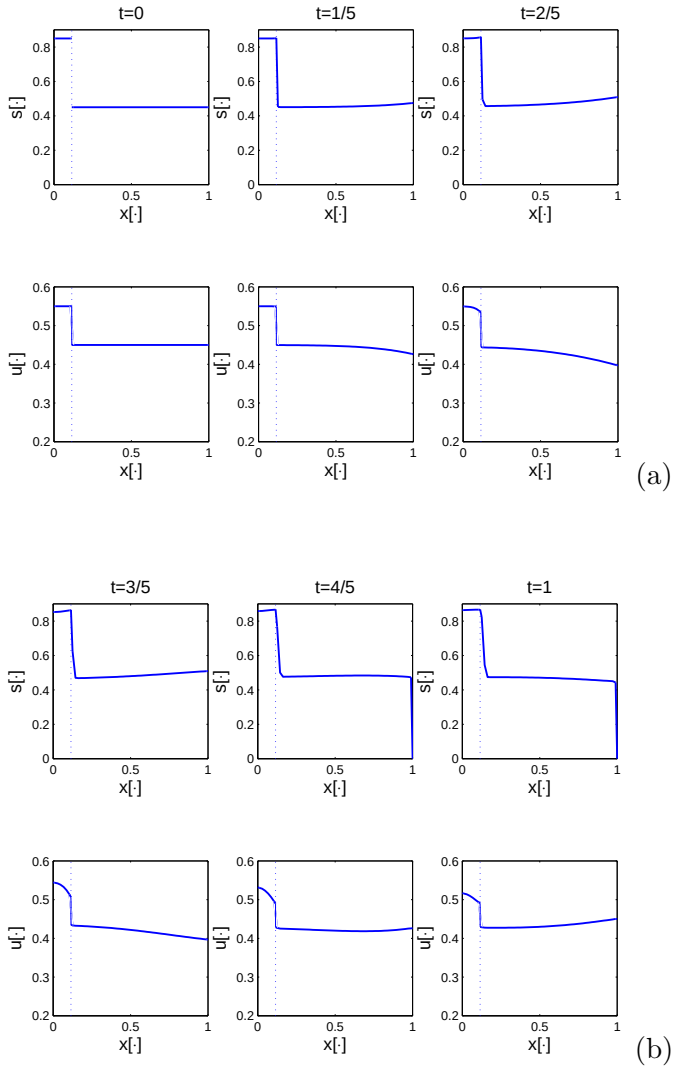

Figure 10. Computational results of Example 2 (s-upwind method): distribution of s and u at different times. (a) $t = 0, 1/5$ and $2/5$. (b) $t = 3/5, 4/5$ and 1.

In order to understand some fundamental properties of this system, the type of boundary conditions needed, the qualitative properties of the solutions etc., we have untangled parabolic and hyperbolic parts by means of a suitable transformation. To illustrate the analytical results we have employed two numerical methods to compute two numerical examples. One of them is front tracking method, which produces the exact shape of the propagating shock in the saturation.

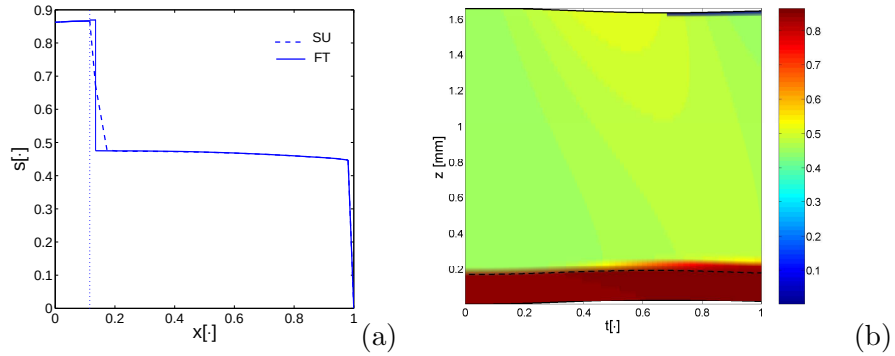

Figure 11. Example 2. (a) Final distribution of saturation s computed by s-upwind and front tracking methods. (b) Saturation in spatial coordinates.

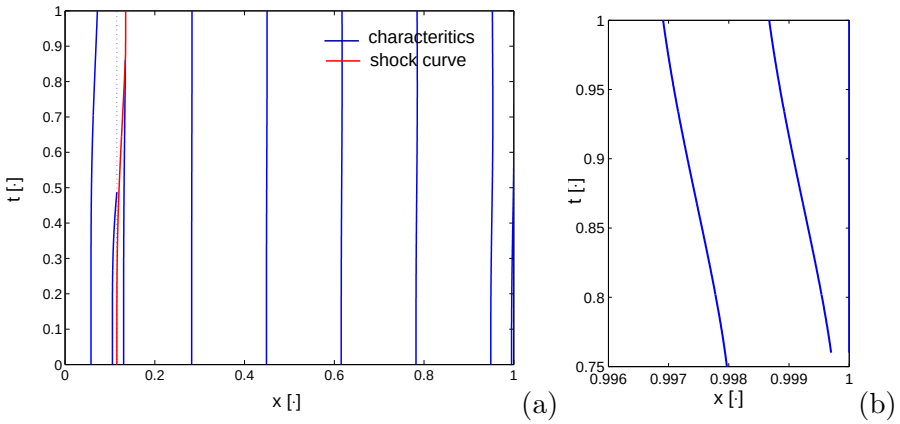

Figure 12. Computed characteristics in Example 2. A) Whole domain. B) Relatively enlarged region near the right boundary.

The simplifying assumption of air incompressibility helps to understand the mathematical behaviour of the system, but it limits direct applications of the results. For this reason we consider the compressible air case in the second part of this paper, using the techniques and results from this study.

Acknowledgements

This work was supported by the Netherlands Organization for Scientific Research (NWO), through the project 613.002.046.

References

Bear, J.: 1972, *Dynamics of Fluids in Porous Media*. Elsevier, New York, 1972.

Bežanović, D., Duijn, C.J. van and Kaasschieter, E.F.: 2003, A three-phase model for wet pressing of paper. *The Proceedings of 2003 International Paper Physics Conference*, 333–336, 2003.

Bežanović, D., Duijn, C.J. van and Kaasschieter, E.F.: 2004, Analysis of paper pressing: the saturated one-dimensional case. To appear in *Journal of Applied Mathematics and Mechanics*.

Bežanović, D., Duijn, C.J. van and Kaasschieter, E.F.: 2005, Analysis of wet pressing of paper: the three-phase model. Part II: compressible air case. (in preparation).

Duijn, C.J. van, Molenaar, J. and de Neef, M.J.: 1995, The effect of capillary forces on immiscible two-phase flow in heterogeneous porous media. *Transport in Porous Media*, **21**, 71–93, 1995.

Friedman, A.: 1964, *Partial Differential Equations of Parabolic Type*. Prentice-Hall, Englewood Cliffs, 1964.

Helmig, R.: 1997, *Multiphase Flow and Transport Processes in the Subsurface*. Springer-Verlag, Berlin, 1997.

Hiltunen, K.: 1995, *Mathematical Modelling for Consolidation Process in Paper Machines*. PhD thesis, University of Jyväskylä, Finland, 1995.

Kataja, M., Hiltunen, K., Timonen, J.: 1992, Flow of water and air in a compressible porous medium. A model of wet pressing of paper. *J.Phys.D: Appl. Phys*, **25**, 1053–1063, 1992.

Ladyzhenskaya, O.A., Solonnikov, V.A. and Uraltceva, N.N.: 1968, *Linear and Quasilinear Equations of Parabolic Type*. Amer. Math. Soc. Transl. Math. Mono 23, Providence, R.I., 1968.

Leveque, R.J.: 1999, *Numerical Methods for Conservation Laws*. Birkhauser Verlag, 1999.

Lewis, R.W., Schrefler, B.A.: 1998, *The Finite Element Method in the Static and Dynamic Deformation and Consolidation of Porous Media*. John Wiley and Sons Ltd, Chichester, 1998.

Renardy, M.: 1996, On an equation describing the spreading of surfactants on thin films. *Nonlinear Anal.*, **26**, 1207–1219, 1996.

Renardy, M.: 1997, A degenerate parabolic-hyperbolic system modeling the spreading of surfactants. *Siam J. Math. Anal.*, **28**(5), 1048–1063, September 1997.

Mulder, B.M.P. and Riepen, M.:, 1994, Wet press modelling, a one-dimensional approach. Report to Netherlands Agency for Energy and Enivironment, project nr. 96.13.6.3201, 1994.

Paulapuro, H.: 2001, Wet pressing-present understanding and future challenges. 12th Fundamental Research Symposium, Oxford, 2001.

Singh, K.M.: 1994, *Mathematical Analysis of the Wet Pressing of Paper*. PhD thesis, SUNY College of Environmental Science and Forestry, Syracuse, New York, 1994.

Smoller, J.: 1980, *Shock waves and reaction-diffuion equations*. Springer-Verlag, New York, 1980.

Ta-tsien, L., Wen-Tzu, Y. and We-shi S.: 1981, Boundary value problems and free boundary problems for quasilinear hyperbolic-parabolic coupled systems. Technical Summary Report 2273, University of Wisconsin, September 1981.

Velten, K. and Best, W.: 2002, Rolling of unsaturated porous materials: Evolution of fully saturated zone. *Physical Review E*, Volume **62**(3), 3891–3899, 2002.